ORIGINAL PAPER

CRYSTAL Research&Technology

www.crt-journal.org

The Bonding Interactions in Fluorinated Vinylogous Amides: A CF_3-Substituted Carbonyl-β-Aminoenone as a Case Study

Edeimis Espitia Cogollo, Eliana Jios, Alejandra Hidalgo, Sonia Elizabeth Ulic, Gustavo Alberto Echeverría, Oscar Enrique Piro, and Jorge Luis Jios**

A new perfluoromethylated vinylogous amide, (Z)-4,4,4-trifluoro-1-(2-hydroxyphenyl)-3-(2-methoxyethylamino)-2-buten-1-one, is chosen as an example to investigate the bonding interactions in solid state. The Z, s-*cis* form is the dominant conformation in both solution and solid state. Intramolecular hydrogen bonding determines this conformational preference in a nonpolar solvent (NMR spectra). Carbonyl and phenol groups are sensitive to the intra- and intermolecular contacts (vibrational spectra). The supramolecular assembly (X-ray diffraction) is governed by NH···O and OH···O strong intermolecular hydrogen bonds giving rise to center-symmetric $R_2^2(16)$ and $R_2^2(12)$ graph-set motifs. The π-stacking, F···H and F···F interactions are also discussed (Hirshfeld analysis).

1. Introduction

The β-trifluoromethyl β-aminoenones, compounds with the general formula: RNH-C(CF_3)=CH—C=O, are very attractive not only from a structural insight, but also because they are interesting and versatile building blocks for medicinal chemistry.[1] Aminoenones are widely used for the synthesis of heterocycles bioactive and analogs of naturally occurring compounds.[1,2]

Considering the main skeleton of (*Z*)-4,4,4-trifluoro-3-(2-metoxyethylamino)-1-(2-hydroxyphenyl)-2-buten-1-one (**1**) as a β-aminoenone (β-ketoenamine), it could belong to the so-called "push–pull olefins". When an electron withdrawing group (EWG) in the α-carbon atom of the olefin like trifluoromethyl is taken into account, the compound becomes a "capto-dative olefin".[1,2] Both properties in the same unit reveal a molecule with a varied and high chemical reactivity. The particular properties of the fluorine atom, such as strong electronegativity, small size and the low polarizability of the C—F bond, impact on the behavior of a molecule in a biological environment, being the H/F interchange one of the most employed monovalent isosteric replacements in drug design.[3,4] The trifluoromethyl group is a very lipophilic, metabolically stable bioisostere for methyl and chloro-groups and also can alter biological processes such as the binding with enzyme or receptor.[5–10] Recently, trifluoromethyl-substituted compounds were shown to have high activity against the malaria parasite.[11] This group is seen as a hard electronegative acceptor group, but close contact between CF_3 groups are commonly found in the Cambridge Structural Database (CSD). As was stated such interactions can be rationalized by assuming a certain degree of polarizability for this group that allows it to interact favorably.[12] Chemically, the —CF_3 bonded to the C-2 olefinic carbon of trifluoromethylchromones transforms the pyran heterocycle into a better Michael acceptor. That is one of the reasons why the title compound is obtained in mild reaction conditions without catalyst, by 1,4-adittion of methoxy 2-aminoethane to 2-trifluoromethylcromone. The attractiveness of this skeleton is complemented by its structural flexibility and resonance across the conjugated double bond connecting the amino and carbonyl groups. Aminoenones are vinylogous amide compounds[13] so that a restriction around the bonds in addition to conformational and tautomerism equilibria, is expected. These molecules can establish strong intramolecular hydrogen bonds N—H···O=C. The main conformation and isomeric forms are depicted in **Scheme 1** using the s-*cis*/s-*trans* designation, applied in dienes to describe the orientation of both unsaturated bonds with respect to the intermediate single "s" bond, adopted for enamine systems.[2,13] For the present example the *cis*/*trans* terminology is not strictly correct, since there are no two equal groups (or hydrogen) around the single bond used as reference.

E. Espitia Cogollo, E. Jios, A. Hidalgo, Prof. S. E. Ulic
CEQUINOR (CONICET-UNLP), Facultad de Ciencias Exactas
Universidad Nacional de La Plata
Bv. 120 N° 1465, La Plata 1900, Argentina
E-mail: sonia@quimica.unlp.edu.ar
Prof. S. E. Ulic
Departamento de Ciencias Básicas
Universidad Nacional de Luján
Rutas 5 y 7, 6700 Luján Buenos Aires, Argentina
Prof. G. A. Echeverría, Prof. O. E. Piro
Departamento de Física, Facultad de Ciencias Exactas
Universidad Nacional de La Plata e IFLP (CONICET, CCT-La Plata)
C. C. 67, La Plata 1900, Argentina
Prof. J. L. Jios
Laboratorio UPL (UNLP-CIC)
Camino Centenario e/505 y 508, M.B. Gonnet, Buenos Aires 1897, Argentina
E-mail: jljios@quimica.unlp.edu.ar
Prof. J. L. Jios
Departamento de Química, Facultad de Ciencias Exactas
Universidad Nacional de La Plata
47 esq. 115 La Plata 1900, Argentina

The ORCID identification number(s) for the author(s) of this article can be found under https://doi.org/10.1002/crat.202000162

DOI: 10.1002/crat.202000162

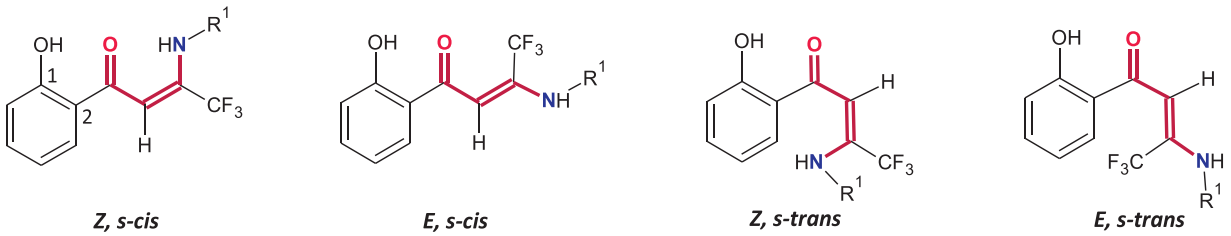

Scheme 1. Main configuration and conformation forms around the C═C─C═O fragment in aminoenones.

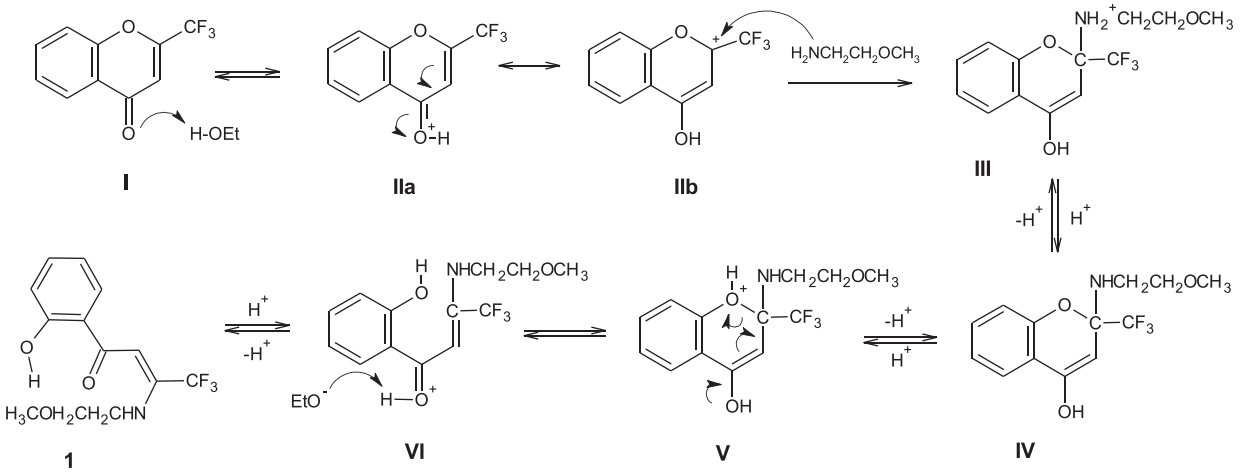

Scheme 2. Synthesis of **1** via nucleophilic addition and heterocyclic ring opening in protic solvent.

In related trifluoromethyl *N,N*-disubstituted aminoenones, the calculated energy difference between the E, s-*cis* and E, s-*trans* structures is less than 2 kcal/mol.[2] Although the most stable conformation in "push–pull" aminoenones without hydrogen atom at the amino group is the *E, s-cis*,[2,13] the presence of an acidic hydrogen (N-H or NH_2) strongly shifts the equilibria between both species to the Z, s-*cis* isomer. This class of compounds are present as individual anancomers as established in closely related compounds.[14–16] Even more, the stable conformation generated by this intramolecular hydrogen interaction was exploited to synthesize Z-selective amides, mediated by a stereo selective reaction pathway.[17] According to the extended resonance in push–pull aminoenones [RNH─C(CF_3)═CH─C═O ↔ RN^+H ═C(CF_3) ═CH═CO^-], a combination of E/Z and *cis*/*trans* forms involving sp^2 hybridized atoms are possible (Scheme 1).

In this work, the title compound was obtained by nucleophilic addition of methoxyethylamine to chromone **I** followed with pyran ring opening in a polar protic solvent (ethanol). **Scheme 2** shows a plausible mechanism for the synthesis of the vinylogous amide derivative **1**.

The inductive effect of the ─CF_3 group in **I** increases the nucleophilicity of C-2. Furthermore, the protic solvent acts as a catalyst promoting the carbocation resonance structure **IIb** and favoring the addition of the amine (**III**). After proton exchange (**IV–V**) the heterocyclic ring opens (**VI**) with the formation of the phenolic group. The last step yields compound **1** and the solvent recovers its proton.

The compound **1** was selected as an example to analyze its tautomeric and conformational equilibria. Nuclear magnetic resonance (NMR) and UV–vis spectroscopy techniques were employed to evaluate the molecule in solution, whereas the conformational preference and intermolecular bonding interactions in solid state were investigated by vibrational spectroscopies (IR and Raman) and single crystal X-ray diffraction spectroscopy. The structural study was complemented with theoretical calculations, which results were compared with the experimental ones and were used to assist the assignment of vibrational spectra.

2. Experimental Section

2.1. Synthesis and Characterization of (Z)-4,4,4-Trifluoro-3-(2-Methoxyethylamino)-1-(2-Hydroxyphenyl)-2-Buten-1-One (1)

Compound **1** was prepared according to a reported procedure[18] but dissolving reactants in ethanol.[14] The yellow crystalline solid, re-crystallized twice in hexane (m.p. 104–105 °C) was suitable for the spectroscopic studies. Adequate single crystals for structural X-ray diffraction were obtained from slow evaporation at 20 °C of concentrated hexane solutions.

^{1}H NMR: δ = 12.76 (1H, s, OH); 10.5 (1H, br.s, NH); 7.66 (1H, dd, J = 7.5 and 2 Hz, H-6); 7.39 (1H, ddd, J = 8, 7 and 2 Hz, H4); 6.95 (1H, dd, J = 8 and 1 Hz, H-3); 6.85 (1H, ddd, J = 8, 7 and 1 Hz, H-5); 6.22 (1H, s, C─H methine); 3.60 (2H, br.s, CH_2─N); 3.59 (2H, s, CH_2─O) and 3.45 ppm (3H, s, CH_3). ^{13}C NMR: δ = 194.0 (C═O); 162.6 (C-1); 150.2 (C-CF_3, q, $^2J_{C,F}$ = 31 Hz); 135.2 (C-3); 128.4 (C-5); 120.3 (C-6), 120.2 (CF_3, q, $^1J_{C,F}$ = 278 Hz); 118.9 (C-4); 118.7 (C-2); 88.4 (vinyl, q, $^3J_{C,F}$ = 3 Hz); 71.0 (CH_2-O); 59.3

(CH_3) and 44.5 ppm (CH_2—N, q, $^4J_{C,F}$ = 3 Hz). ^{19}F NMR: δ = -67.0 ppm. UV–vis: λ max (nm) 365, 262, and 221.

2.2. Instrumentation

2.2.1. Infrared and Raman Spectroscopy

Infrared spectra of **1** in KBr pellets were recorded on a LUMEX Infra LUM FT-02 spectrometer with a resolution of 2 cm^{-1} in the range from 4000 to 400 cm^{-1}. Raman spectra of the solid (at room temperature) were measured in Pyrex standard capillaries (2.5-mm i.d.) on a Bruker IFS 66 spectrometer (spectral resolution 4 cm^{-1}), equipped with a 1064 nm Nd:YAG laser, in the range from 4000 to 100 cm^{-1}.

2.2.2. NMR Spectra

The ^{1}H (200.0 MHz), ^{19}F (188.7 MHz) and ^{13}C (50.3 MHz) NMR spectra of **1** were recorded at 298 K on a Varian Mercury Plus 200 spectrometer. The sample was dissolved in $CDCl_3$ in a 5 mm NMR tube. Chemical shifts, δ, for ^{13}C and ^{1}H NMR spectra are given in ppm relative to TMS (δ = 0 ppm) and are referenced by using the residual non deuterated solvent signal. For ^{19}F NMR spectrum, a 0.05% TFA in $CDCl_3$ solution was used as external reference (δ = −71.0 ppm). Coupling constants, *J*, are reported in Hz, and multiplicities are denoted as: s (singlet), dd (double doublet), ddd (double double doublet), q (quartet), and br.s (broad singlet). The atom numbering shown in Scheme 1 was adopted to facilitate the comparison with data reported in the literature.

2.2.3. UV–Visible Spectroscopy

The spectra of **1** in methanol were recorded using a quartz cell (10 mm optical path length) on a Chrom Tech CT-5700 UV/Vis spectrophotometer, with 2.0 nm spectral bandwidth. Measurements were carried out in the spectral region from 190 to 700 nm.

2.2.4. X-Ray Diffraction Data

The measurements were performed on an Oxford Xcalibur Gemini, Eos CCD diffractometer with graphite-monochromated CuKα (λ = 1.54184 Å) radiation. X-ray diffraction intensities were collected (ω scans with ϑ and κ-offsets), integrated and scaled with CrysAlisPro[19] suite of programs. The unit cell parameters were obtained by least-squares refinement. The unit cell parameters were obtained by least-squares refinement (based on the angular settings for all collected reflections with intensities larger than seven times the standard deviation of measurement errors) using CrysAlisPro. Data were corrected empirically for absorption employing the multi-scan method implemented in CrysAlisPro. The structure was solved by direct methods with SHELXS of the SHELX suite of programs[20] and the molecular model refined by full-matrix least-squares procedure on F^2 with SHELXL of the same package. ORTEP-3[21] and Mercury[22] programs were used for molecular graphics.

The hydrogen atoms were positioned stereo-chemically and refined with the riding model. The methyl and hydroxyl groups' angular locations were optimized during the refinement by treating them as rigid bodies which were allowed to rotate around the O—CH_3 and C—OH bonds, respectively. The CH_3 group converged to a staggered position and the OH one onto the molecular plane. Crystal data, structure refinement results and structural parameters of **1** are summarized in Table S1, Supporting Information and have been deposited at the Cambridge Crystallographic Data Centre (CCDC). Any request to the CCDC for this material should quote the full literature citation and the reference number CCDC 2014031.

2.3. Computational Methods

Theoretical calculations were performed using the program package Gaussian 03.[23] Scans of the potential energy surface, optimizations, and vibrational frequency calculations of possible conformers of **1** were carried out with the density functional theory (B3LYP) method,[24–26] employing the 6-311++G(d,p) basis set. The calculated vibrational properties correspond, in all cases, to potential energy minima with no imaginary values for the frequencies. The theoretical electronic spectrum was predicted with TD-DFT (B3LYP/6-311++g(d,p)), and the polarizable continuum model (PCM) was used to consider the solvent effect (methanol).

2.4. Hirshfeld Surface (HS) Calculations

The HS analysis was used to investigate, in detail, the characteristics of the crystal packing. HS and their associated 2D fingerprint plots (2D FP) were performed using the CrystalExplorer17 program.[27] The structural parameters of **1** were taken from the CIF file.

The 3D d_{norm} (normalized contact distance) surface was mapped over a fixed color scale of −0.1080 au (red) to +0.7070 au (blue) Å. The 2D FP, whose shapes are typical for certain close contacts, were displayed by using the translated 1.0 — 2.8 Å range and including reciprocal contacts. Shape index and curvedness functions were also computed, since they allow for intuitive recognition and visual analysis of interactions between molecules.[28–31]

3. Results and Discussion

3.1. Crystallographic Structural Results

An ORTEP[21] drawing of **1** is shown in **Figure 1** and a selection of inter-atomic bond distances and angles are presented in **Table 1**. As expected, the *o*—HOC_6H_4—C(O)—CH=C(CF_3)—NH-R molecular skeleton is nearly planar (*rms* deviation of non-H atoms from the least square plane of 0.070 Å) since the π-bond delocalization extends throughout the molecular framework. In addition, the O—H···O and N—H···O intramolecular hydrogen bonds reinforce the molecular planarity, being the last interaction also responsible for the observed Z-configuration in the crystalline lattice. The forms **I–II**

Table 1. Selected experimental and calculated bond lengths [Å] and angles [°] for **1**.

Parameters	Exp.	Calc.[a)]	Parameters	Exp.	Calc. [a)]
Bond lengths					
C(1)—O(1)	1.349(3)	1.341	C(8)—C(9)	1.365(4)	1.376
C(1)—C(6)	1.407(4)	1.423	C(9)—N	1.338(4)	1.344
C(6)—C(7)	1.472(4)	1.479	C(11)—N	1.456(4)	1.461
C(7)—O(2)	1.252(3)	1.263	C(12)—O(3)	1.397(4)	1.414
C(7)—C(8)	1.440(4)	1.442	C(13)—O(3)	1.394(4)	1.417
Bond angles					
O(1)—C(1)—C(2)	117.3(3)	117.3	N—C(9)—C(8)	125.2(3)	125.2
O(1)—C(1)—C(6)	122.3(3)	122.7	C(8)—C(9)—C(10)	117.9(3)	117.9
C(1)—C(6)—C(7)	120.1(3)	119.4	N—C(11)—C(12)	110.7(3)	109.7
O(2)—C(7)—C(8)	119.8(3)	120.0	O(3)—C(12)—C(11)	114.8(3)	108.0
O(2)—C(7)—C(6)	119.6(3)	119.1	C(9)—N—C(11)	131.1(3)	129.2
C(9)—C(8)—C(7)	123.1(3)	122.9	C(12)—O(3)—C(13)	115.3(3)	113.6
Torsion angles					
C(2)—C(1)—C(6)—C(7)	−179.5(3)	−180.0	C(8)—C(9)—N—C(11)	−174.2(3)	173.7
C(1)—C(6)—C(7)—C(8)	178.3(3)	179.4	O(1)—C(1)—C(6)—C(5)	179.7(3)	−179.9
C(6)—C(7)—C(8)—C(9)	175.7(3)	−179.6	N—C(9)—C(8)—C(7)	0.7(5)	−1.4
O(2)—C(7)—C(6)—C(1)	−2.3(4)	−0.5	O(2)—C(7)—C(8)—C(9)	−3.7(5)	0.3
N—C(11)—C(12)—O(3)	−64.1(4)	60.4	C(11)—C(12)—O(3)—C(13)	−85.9(4)	−120.5

[a)] [B3LYP/6-311++G(d,p)].

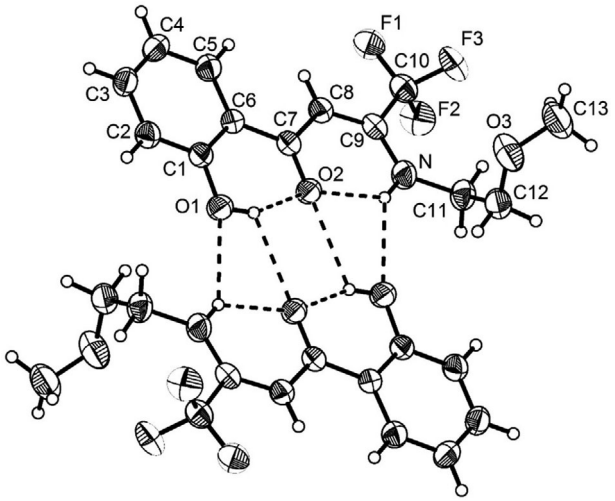

Figure 1. Drawing of dimeric **1**, showing the labeling of the non-H atoms and their displacement ellipsoids at the 30% probability level. The molecules in the dimer are symmetrically related to each other through a crystallographic inversion center. The H-bonding structure is indicated by dashed lines.

and **I–III** (**Scheme 3**) can be interpreted as a part of the Resonance Assisted Hydrogen Bond (RAHB) synergistic π-delocalized model conferring the higher planarity observed for the *o*-hydroxybenzoyl, (HOPh(C=O); *rms* of 0.008 Å) and ketoenamine (—C(O)—CH=C(CF_3)NHCH_2—; *rms* of 0.028 Å) groups. The latter resembles the one that produces peptide bond planarity [—C(=O)—NH— ↔ —C(—O^-)=N^+H-], reinforcing the vinylogy concept since the ketoenamine system acts as an amide vinylogous. Observing the bond distances between the carbonyl atom (C7) and both α-C atoms (C6 and C8), the C7-C8 [d(C—C) = 1.440(4) Å] is shorter than C6-C7 [d(C—C) = 1.472(4) Å]. Although both bonds are affected by charge delocalization according to the RAHB model, the former corresponds to an amide vinylogous that explain its increases in bond character. Because the weaker intramolecular N—H···O hydrogen bond (compared with the O—H···O ones), the enamine moiety depart slightly from co-planarity with a dihedral angle of 6.2(2)°. The overall planar conformation is further stabilized by a pair of strong intra-molecular Ph—OH···O···HN< bonds [O1···O2 and N···O2 distances of 2.540(3) and 2.655(3) Å]. Particularly important is the resonance within the bonding structure of the *o*-hydroxyacetophenone group, HOPh(C=O), and between the C8=C9 [d(C—C)=1.365(4) Å] and C9=N [d(C—N) = 1.338(4) Å] double bonds.

Table 2. Experimental and calculated intramolecular and experimental intermolecular hydrogen bond distances (Å) and angles (°) for **1**.

D—H···A[a,b)]	d(D—H)	d(H···A)	d(D···A)	∠(D—H···A)
Intramolecular				
N—H(0)···O(2)	0.86 (1.02)[b)]	1.98 (1.86)[b)]	2.655(3) (2.664)[b)]	134.0 (132.9)[b)]
O(1)—H(1)···O(2)	0.82 (0.99)[b)]	1.83 (1.64)[b)]	2.540(3) (2.537)[b)]	144.5 (148.1)[b)]
Intermolecular				
N—H(0)···O(1′)[a)]	0.86	2.37	3.101(4)	142.5
O(1)—H(1)···O(2′)[a)]	0.82	2.43	2.908(3)	118.3

[a)] Symmetry code: −x,−y+2,−z [b)] Calculated (B3LYP/6-311++G(d,p)) values in parenthesis.

As shown in Figure 1 and **Table 2**, neighboring (inversion related) molecules in the lattice are arranged as planar dimers, linked through intermolecular N—H···O(1′) and O1—H1···O(2′)

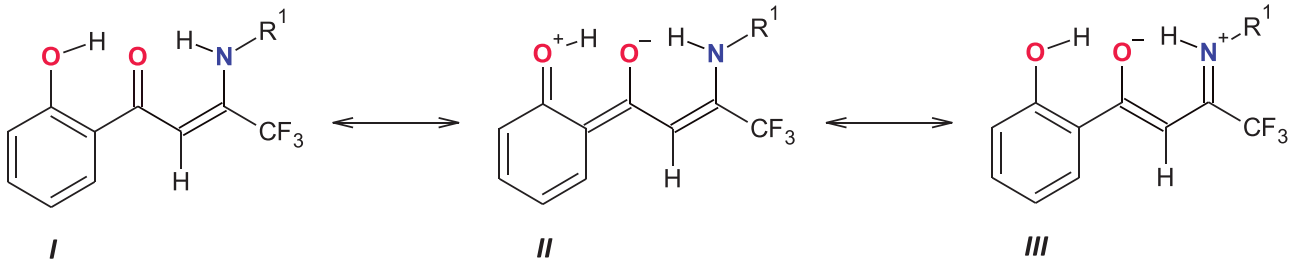

Scheme 3. Representative resonance structures of **1,** showing the π-delocalized electrons across the planar conjugated phenyl – ketoenamine system.

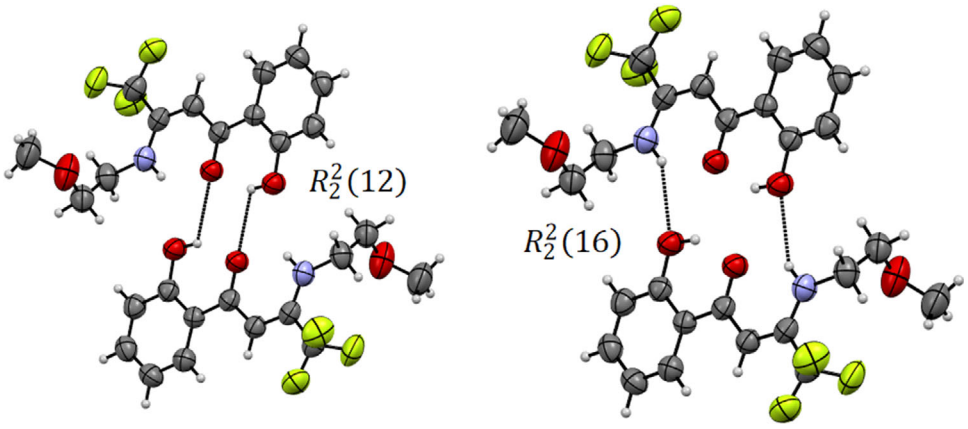

Figure 2. Crystal packing of **1**, showing the $R_2^2(12)$ and $R_2^2(16)$ graph-set motifs. The centre-symmetric dimers are connected by intermolecular hydrogen bonds (dashed lines).

bonds [d(N···O1′) = 3.101(4) Å and d(O1···O2′) = 2.908(3) Å]. The N—H···O(1′) interaction associates neighboring molecules through the N—H amino group and the acceptor oxygen atom of the phenol group, leading to center-symmetric $R_2^2(16)$ dimers in a supramolecular assembly. Besides, the O1—H1···O(2′) contacts link the molecules into a second center-symmetric dimmer originating $R_2^2(12)$ graph-set motifs (see **Figure 2**).

3.2. Quantum Chemical Calculation

The geometrical parameters for the most stable conformation together with the experimental ones are showed in Table 1 for a better comparison. In the calculated structure, three planar moieties (the aromatic ring and two six-atom pseudo-rings connected successively by O—H···C=O and C=O···H—N hydrogen bonds) define a central plane in the molecule. The interatomic distances and angles are in good agreement with the observed ones in the crystal lattice. The carbonyl group is of crucial importance to keep the aforementioned planarity, both in the crystalline network and in the optimized conformation in vacuum. The C—O interatomic distance (exp.: 1.252(3) Å, calc.: 1.263 Å) is characteristic of double bond α, β-unsaturated carbonyl systems, coplanar to both the aromatic and the enamino moieties with O2C7C6C1 and O2C7C8C9 dihedral angles of −2.3(4)° (calc. −0.5°) and −3.7(5)° (calc. 0.3°), respectively.

Moreover, the RAHB model[32] allows explaining the electronic charge delocalization along the bonds in the O=C7—C8=C9—N—H and the O=C7—C6=C1—O—H pseudo rings. The C7—C8 bond (exp. 1.440 Å; calc. 1.442 Å) is shorter than the C6—C7 bond (exp. 1.472 Å; calc. 1.479 Å) distance, suggesting that the charge is more effectively delocalized through the O = C7-C8 = C9-N-H moiety. Regarding to the typical single C—C distance, C6—C7 and C7—C8 show bond order greater than the unity as observed when comparing with C9—C10 and C11—C12 bond distances with values of 1.503 Å (calc.1.525 Å) and 1.504 Å (calc.1.519 Å), respectively.

The calculated intramolecular inter-atomic O1···O2 and O2···N distances and O1···H···O2 and O2···H···N angles, involved in the hydrogen bonds, are 2.537 Å, 2.664 Å, 148.1°, and 132.9°, respectively. Values of 2.540 Å, 2.655 Å, 144.5° and 134.0°, respectively, are obtained from X-ray diffraction analysis (see **Table 2**). This good agreement between theoretical and experimental results highlights the relevance of these interactions, in both solid and gas phase, to stabilize the predicted conformation.

The orientation of the methoxyethyl group with respect to the ketoenamine plane is the main difference when the most stable conformation is compared with the molecule in the crystal. In the optimized structure the alkyl chain is rather out of the plane, while the experimental conformation strongly deviates from the same plane with C9NC11C12 torsion angle values of 15.5° (calc.) and 122.3 (exp.), see Table 1.

3.3. HS Results

The HS of **1** mapped over d_{norm}, presented in **Figure 3**, clarifies the nature and extent of the intermolecular interactions. The short

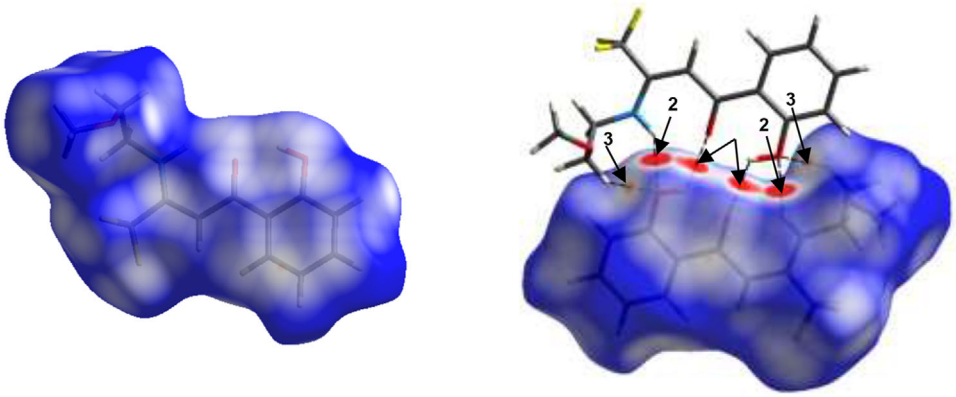

Figure 3. Hirshfeld surfaces (HS) of 1 mapped over d_{norm}. Front (left) and opposite (right) view. See text for labels description.

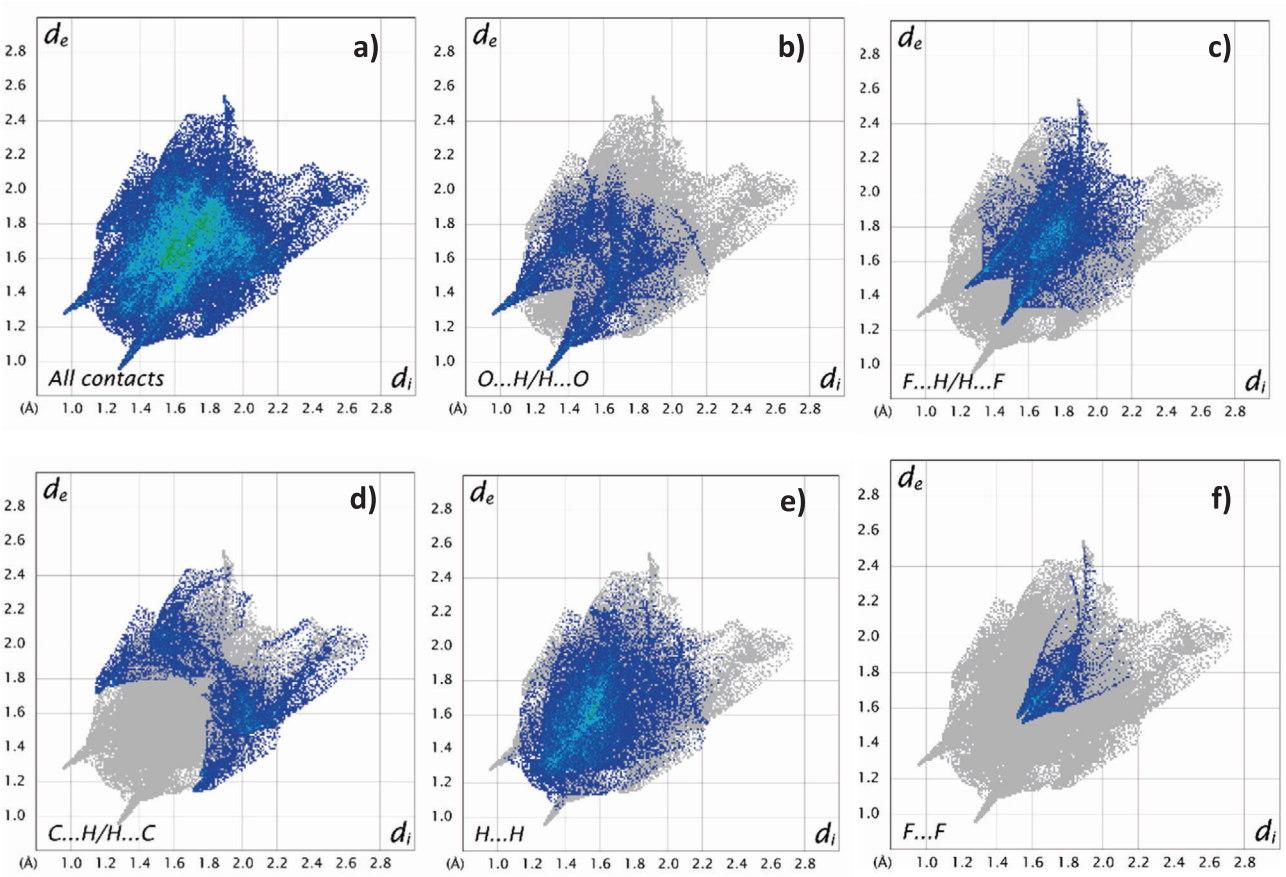

Figure 4. a) 2D Fingerprint plots of all contacts; b) O···H / H···O; c) F···H / H···F; d) C···H / H···C; e) H···H and f) F···F contributions of interactions.

and dominant intermolecular contacts are shown as bright red areas on the HS, indicating the existence of hydrogen bonding (HB) interactions. As was stressed above, the molecules are arranged antiparallel as center-symmetric dimers in the solid to maximize the intermolecular contacts. Although in the HS front view the molecule exhibits no significant interactions, the opposite view (rotated 180° around the plot horizontal axis) shows the most important contacts.

The two strong reciprocal O1—H···O2′ and O2···H—O1′ and O1···H—N′ and N—H···O1′ hydrogen bond interactions are labeled with 1 and 2, respectively, whereas that the two weak O1···H12A—C12′ and C12—H12A···O1′ contacts (small red circles of low intensity, see Figure 3) are displayed as 3.

The 2D FP of **1** are depicted in **Figure 4**, and the relative contribution of the main intermolecular contacts to the HS area is visualized in **Figure 5**. The strong O—H···O hydrogen bond interac-

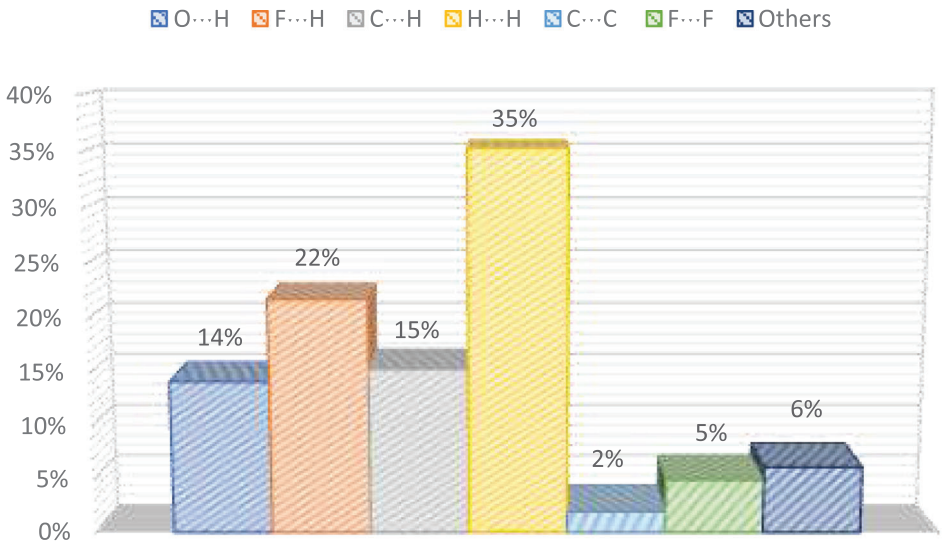

Figure 5. Relative contribution [%] of intermolecular contacts to the HS area of **1**.

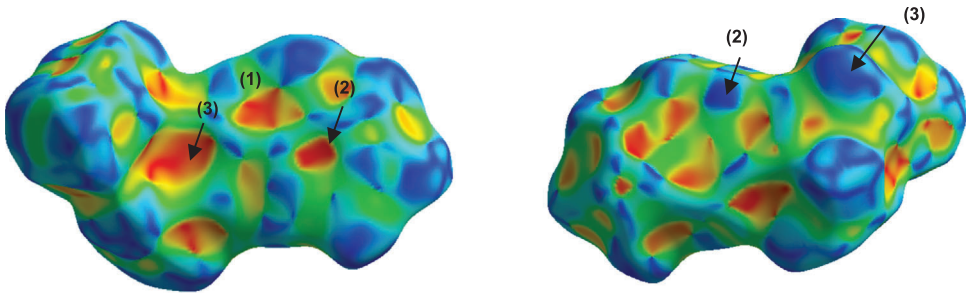

Figure 6. Shape index surface of **1**. Front (left) and back (right) view.

tions are indicated as a pair of quite symmetric narrow spikes at around (d_e+d_i) of 2.05 Å and contribute with 14% to the total HS. Besides, the F···H/H···F contacts show similar 2D FP feature, but with spikes at around (d_e+d_i) of 2.75 Å with 22% contribution to the HS. Crystallographic results evidence F···H interatomic distances of 2.783 Å. Other unconventional contacts such as H···H[33] and F···F,[34,35] which have been reported as not negligible, also promote the stabilization of the molecule in the crystal lattice. The H···H and F···F contacts represent 35% (main contribution) and 5%, respectively, of the total area and fluorine atoms seem to be important in the arrangement of the molecule. In the full FP, that shows all the contacts (Figure 4a), light blue and green areas observed along the diagonal of the graph are indicative of π-stacking interactions, consistent with the FP results for C···H and C···C interactions, and with the percentage of H···H contributions.

Considering the crystallographic results, the interaction between fluorine atoms could be favored since trifluoromethyl groups are stacked side by side and face each other with fluorine atoms belonging to the next row of molecules (Figure S4, Supporting Information). According to recently reported results, close "negative–negative" contacts between CF3 groups occur by polarization of C—F bonds by the field exerted when the atoms approach.[12] In this way the multiple F···F interactions, although weak, can influence the molecular geometry. The shortest F2···F3 interatomic distance found in the crystal was 3.088 Å.

HS is not equivalent on both sides since the molecule is not plane, which is better displayed on the shape index graphs, and the front and back surface views of **1** are shown in **Figure 6**. The red and blue triangles (1) in the front view denote the self-complementary hollow and bump region. It involves the H—O1—C1—C6—C7—O2 pseudo ring of both related inversion center molecules. The intermolecular O1···C7 distance and C1O1C7 angle are 3.38 Å and 107°, respectively, whereas the intermolecular O1···O2 distance is 3.21 Å. These distances are lower than the sum of the vdW radii. A high charge delocalization, supported by resonance assisted hydrogen bond, characterizes the pseudoring.

The pair of complementary contacts (2) is established between the carbonyl oxygen O2 (back view) and the C4—C5 carbons belonging to the phenyl ring (front view). Precisely, the C4-C5 (1.371 Å) is the shorter bond distance of the phenyl ring. The phenyl and the pseudo H—O1—C1—C6—C7—O2 ring are parallel-displaced with an interplanar distance of 3,37 Å, and the intermolecular O2C4 and O2···C5 contacts are 3.59 Å and 3.52 Å, respectively. The Mercury packing diagram[19] allows a better view of the molecules arranged in the stacking (see Figure S5, Supporting Information). The complementary contact (3) is the most

Table 3. Experimental and calculated frequencies (cm^{-1}) and assignment of the fundamental vibrational modes of **1**.

Experimental[a]		Calculated[b]		Assignment[f]
IR[c]	Raman[d]	Frequency[a]	Intensity[e]	
3164 (vw)	3131 (4)	3300	514 (14)	ν(O1—H)
1623 (vs)	1622 (60)	1659	587 (8)	ν(C7═O2); ν(C═C)$_{ar}$
1363 (m)	1356 (60)	1390	88 (56)	δ(N—H); ν_{as}(C8—C9—N)
1304 (vs)	1304 (43)	1337	151 (13)	ν(C1—O1)
1191 (s)	1193 (8)	1205	125 (4)	$\nu_s(CF_3)$; ν_{as}(C9—N—C11)
1146 (m)		1148	109 (2)	$\nu_{as}(CF_3)$; δ(C—H)$_{ar\text{-}oph}$
1131 (vs)	1130 (7)	1146	244 (1)	ν_{as}(C12—O3—C13)
1085 (m)	1085 (6)	1111	295 (<1)	$\nu_{as}(CF_3)$
971 (w)	972 (6)	977	28 (4)	ν_s(C12—O3—C13)
817 (s)	822 (25)	831	112 (<1)	γ(O—H)
787(vvw)	778 (1)	808	13 (<1)	γ(N—H)

[a] In cm^{-1} [b] B3LYP 6-311++g (d,p) [c] vs, very strong; s, strong; w, weak; vw, very weak; sh, shoulder [d] Raman relative intensities, in parentheses [e] Calculated IR Intensities in km mol^{-1}, and calculated Raman intensities between parentheses [f] ν, δ, γ, represent stretching, in plane deformation, out-of-plane deformation modes, respectively.

visible, with large and deep red/blue zones. It shows the C···H interaction between the C8-C9 carbon atoms (front view) and the H11B hydrogen (back view). The intermolecular distances of C8···H11B and C9···H11B contacts are 3.05 Å and 2.98 Å, respectively. Considering the interatomic distances within the pseudo ring, the C8—C9 bond is the shorter C—C bond with a higher double bond character that could explain the intensity of this interaction. The π···π stacking interactions are better observed in the Curvedness surface representation. The front and back view plots of **1** are characterized by broad and relatively flat areas surrounding the phenyl and the resonance assisted hydrogen bond pseudo rings (Figure S5, Supporting Information).

3.4. Vibrational Spectra

The IR and Raman tentative assignment of the most relevant vibrational modes for the characteristic functional groups (observed and computed frequencies) are presented in **Table 3** (See experimental spectra and complete vibrational modes assignment of **1** in Figure S7 and Table S6, Supporting Information).

This new β-aminoenone (**1**) has C_1 symmetry and all normal vibrational modes are active in both IR and Raman. The very weak IR band observed at 3164 cm^{-1} and at 3131 cm^{-1} in Raman (calc. 3300 cm^{-1}) is attributed to the OH group. Considering that the free O—H stretching vibration in phenols is detected as sharp bands in the region of 3700–3600 cm^{-1} in the gas phase, the low frequency observed for this vibration in **1** indicates its participation in HB interactions. The HB is evidenced by the remarkable red shift of the O—H stretching band. An intramolecular hydrogen bond is highly favored when, as a consequence of the interaction, a 5- or 6-membered pseudo ring structure is generated.[36–38]

The Raman band at 1356 cm^{-1} is attributed to the OH in plane bending, and the strong IR band at 817 cm^{-1} (Raman 822 cm^{-1}) to the out-of-plane bending mode. The position of this band (blue shifted) also evidenced the participation of the O—H group in the HB interactions.

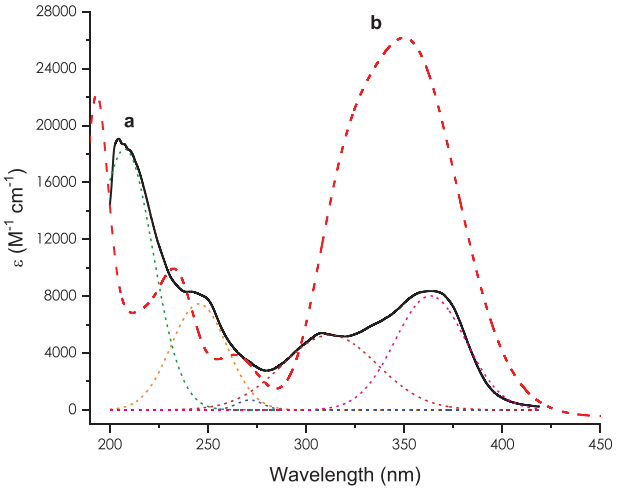

Figure 7. a) Experimental (Gauss fitted) and b) calculated electronic spectra of **1**.

The N—H stretching band was not observed in both spectra, probably because of its low intensity. The in plane deformation of the N—H group can be attributed to the band at 1363 cm^{-1} (IR) and 1356 cm^{-1} (Raman), and the out-of-plane bending, expected at 808 cm^{-1}, is assigned to the very weak IR band at 787 cm^{-1} (Raman: 778 cm^{-1}) and in accordance with reported values of related compounds.[39,40]

The ν(C═O) stretching is assigned to the very strong IR band at 1623 cm^{-1} and to the weak absorption at 1622 cm^{-1} in Raman (Calc. 1659 cm^{-1}). The location of this mode reveals its involvement in intra and intermolecular interactions. Moreover, the C═O stretching is strongly coupled with the ν(C8 = C9), which is expected at 1662 cm^{-1}, as observed in related compounds.[41]

The strong IR absorption at 1304 cm^{-1} is attributed to the C═O stretching of the phenyl group, whereas that the corresponding to the methoxy moiety can be described as asymmetric and symmetric stretchings at 1131 and 971 cm^{-1}, respectively.

The IR bands located at 1191, 1146, and 1085 cm^{-1} (Calc.: 1205, 1148 and 1111 cm^{-1}) are assigned to the $\nu_s CF_3$, $\nu_{as} CF_3$ and $\nu_{as} CF_3$, respectively.

Moreover, the δ(C1–C6–C7) deformation mode of aliphatic moiety is attributed to the Raman band at 385 cm^{-1}. No infrared counterpart was observed, since the band is located out of the spectrophotometer measurement range.

3.5. Electronic Spectra

Calculated and experimental (2.45 10^{-5} M) electronic spectra of **1**, using methanol as solvent, are shown in **Figure 7**. The wavelengths and the oscillator strengths of the observed bands, the corresponding calculated values, and a tentative assignment of the electronic transitions of **1** are presented in **Table 4**. The oscillator strength (*f*) is a valuable parameter associated to the intensity of the transitions, and it can be calculated from the experimental molar extinction coefficients (ϵ) (see Figure S8, Supporting Information).[42] TD-DFT calculations also provide the values of *f*,

Table 4. Experimental and calculated electronic spectra and tentative assignment of most relevant electronic transitions of **1**.

Experimental		Calculated[b]			
λ [nm]	f[a]	λ [nm]	f[c]	Assignment	%
210	0.430	193	0.357	HOMO-3 → LUMO + 2	68
241	0.191	234	0.158	HOMO-1 → LUMO + 2	96
273	0.010	265	0.071	HOMO-3 → LUMO	80
308	0.143	323	0.283	HOMO-1 → LUMO	91
364	0.120	358	0.398	HOMO → LUMO	93

[a] $f = 4.32 \cdot 10^{-9} \int \epsilon d\upsilon$ [b] B3LYP/6-311++g(d,p) [c] Oscillator strength in atomic units

which were considered for the observed absorptions assignment. Particularly, for some transitions the experimental and calculated values fit well, and only the dominant transitions ($f > 0.1$) were considered to assign the observed bands (the main molecular orbitals involved in the electronic transitions are depicted in Figure S9, Supporting Information). The intense absorption observed at 210 nm is generated by the contribution of one electron transitions HOMO-3 → LUMO+2 (calc. 193 nm), and corresponds to excitations from π orbitals of the phenyl ring and non-bonding orbitals of the carbonyl oxygen atom to π^* of the aromatic moiety. The band at 241 nm arise from HOMO-1 → LUMO+2 transitions (calc. 234 nm), and it is mainly dominated by $\pi \rightarrow \pi^*$ transitions involving the phenyl ring with a contribution of non-bonding orbitals of both oxygen and nitrogen atoms.

The absorptions at 273, 308 and 364 nm (Calc. 265, 323 and 358 nm) are originated by HOMO-3 → LUMO, HOMO-1 → LUMO+2, and HOMO →LUMO excitations, respectively. These bands are substantially dominated by $\pi \rightarrow \pi^*$ excitations within the aromatic fragment, with the participation of π orbitals of C═C bond and non-bonding orbitals of the oxygen and nitrogen atoms.

The calculated Δ(HOMO-LUMO) energy gap for **1** was 3.9620 eV, a value that is in very good agreement with that found for (Z)-4,4,4-trifluoro-1-(2-hydroxyphenyl)-3-(methylamino)-2-buten-1-one.[14]

3.6. NMR Spectra

The ^{1}H, ^{13}C, and ^{19}F NMR spectra (Figures S1–S3, Supporting Information) are consistent with the presence of a single species in $DCCl_3$ solution (only one set of signals was detected). The analysis of tautomers that can exist in equilibrium for related aminoenones revealed that only one of the tautomeric forms is predominant in solution.[14,15] NMR spectra indicate that the conformation of **1** is Z, s-*cis* (scheme 1). This structure is shaped by the resonance contributors represented in Scheme 2. The two most deshielded signals at 12.76 and 10.5 ppm in the ^{1}H NMR were assigned to the protons linked to the phenol and amino groups, respectively, which are also bonded to the same carbonyl oxygen acceptor, showing a strong intramolecular interaction. In comparison with the results in solid state in nonpolar solvents, the absence of possible interactions with the solvent reinforces the intermolecular HB. The singlet at 6.22 ppm, that integrates for one hydrogen atom, has a diagnostic value since it confirms the existence of the methine group in the pseudo ring of the β-enamino keto tautomer.

The most deshielded ^{13}C NMR signal at 194.0 ppm, assigned to the carbonyl carbon atom, is influenced by both the hydrogen bond and the RAHB effect. The methine signal at 88.1 ppm confirms the aminoenone tautomer. The singlet at −67.0 ppm in the ^{19}F NMR spectrum is close to the values found for (Z)-4,4,4-trifluoro-3-(2-hydroxyethylamino)-1-(2-hydroxyphenyl)-2-buten-1-one and (Z)-4,4,4-trifluoro-1-(2-hydroxyphenyl)-3-(methylamino)-2-buten-1-one.[14,15]

4. Conclusions

In this work, the perfluoromethylated amide vinylogous (Z)-4,4,4-trifluoro-1-(2-hydroxyphenyl)-3-(2-methoxyethylamino)-2-buten-1-one **1** was taken as a case study to investigate its behavior, and extend it to this class of compounds, in the crystalline lattice and in solution. It also highlights how decisive the hydrogen bond and other weak interactions are in the final conformation adopted for the molecule. The Z, s-*cis* configuration was the only form found in the crystal. The molecule is nearly planar due to the extensive π-conjugation and the intramolecular hydrogen bonds involving the phenol ring and the enamine moiety. They form two pseudo rings with the same acceptor carbonyl oxygen atom. The same donating and acceptor groups participate in the supramolecular assembly forming center-symmetric dimers. This class of stacking was found in a related molecule, leading to a common pattern for such compounds. The interatomic distances in both pseudo rings are affected by the charge delocalization according to the RAHB model, but the single bond between the carbonyl and the α-vinyl carbon atoms is shorter than the distance with the opposite α-carbon atom of phenyl ring. The high bond order character found for the former was explained based on the amide vinylogous concept. In addition, vibrational spectra were sensitive for monitoring the intra- and intermolecular contacts. Particularly, the carbonyl and hydroxyl groups show absorption wavenumbers that indicate strong HB interactions. The electronic spectra show that the bonding and antibonding orbitals of the aromatic ring are mostly involved in the most significant electronic transitions of **1**. The intramolecular hydrogen bonds are also decisive when **1** is dissolved in aprotic solvent, since the only form observed is also the Z, s-*cis*, as confirmed by NMR spectra.

Supporting Information

Supporting Information is available from the Wiley Online Library or from the author.

Acknowledgements

This work was supported by ANPCyT (PICT 2016-0226), CONICET (Grant Nos. PIP 11220130100651 CO, PIP 0359), and UNLP (Grant Nos. 11/X709, 11/X830, and 11/X848) of Argentina. G.A.E., O.E.P., and S.E.U. are research fellows of CONICET. J.L.J. is a research fellow of Comisión de Investigaciones Científicas de la Prov. de Buenos Aires (CIC).

Conflict of Interest

The authors declare no conflict of interest.

Keywords

Hirshfeld analysis, hydrogen bonding, vinylogous amide, X-ray diffraction

Received: August 18, 2020
Revised: December 5, 2020
Published online: December 22, 2020

[1] U. Kuckländer, in *The Chemistry of Enamines* (Ed: Z. Rappoport), The Chemistry of Functional Groups, John Wiley & Sons, Chichester, UK **1994**, pp. 523–636.
[2] E. V. Kondrashov, L. P. Oznobikhina, T. N. Aksamentova, N. N. Chipanina, A. R. Romanov, A. Y. Rulev, *J. Phys. Org. Chem.* **2016**, *29*, 288.
[3] G. A. Patani, E. J. LaVoie, *Chem. Rev.* **1996**, *96*, 3147.
[4] W. K. Hagmann, *J. Med. Chem.* **2008**, *51*, 4359.
[5] A. Y. Rulev, *Eur. J. Org. Chem.* **2018**, *2018*, 3609.
[6] R. Wilcken, M. O. Zimmermann, A. Lange, A. C. Joerger, F. M. Boeckler, *J. Med. Chem.* **2013**, *56*, 1363.
[7] B. E. Smart, *J. Fluorine Chem.* **2001**, *109*, 3.
[8] K. Müller, C. Faeh, F. Diederich, *Science* **2007**, *317*, 1881.
[9] J.-P. Bégué, D. Bonnet-Delpon, *J. Fluorine Chem.* **2006**, *127*, 992.
[10] B. M. Johnson, Y.-Z. Shu, X. Zhuo, N. A. Meanwell, *J. Med. Chem.* **2020**, *63*, 6315.
[11] C. Upadhyay, M. Chaudhary, R. N. De Oliveira, A. Borbas, P. Kempaiah, P. Singh, B. Rathi, *Expert Opin. Drug Discovery* **2020**, *15*, 705.
[12] C. Esterhuysen, A. Heßelmann, T. Clark, *ChemPhysChem* **2017**, *18*, 772.
[13] E. Kleinpeter, A. Schulenburg, I. Zug, H. Hartmann, *J. Org. Chem.* **2005**, *70*, 6592.
[14] M. Rocha, D. M. Gil, G. A. Echeverría, O. E. Piro, J. L. Jios, S. E. Ulic, *J. Fluorine Chem.* **2018**, *208*, 36.
[15] A. Hidalgo, L. P. Avendaño Jiménez, L. A. Ramos, M. A. Mroginski, J. L. Jios, S. E. Ulic, G. A. Echeverría, O. E. Piro, E. Castellano, *J. Phys. Chem. A* **2012**, *116*, 1110.
[16] N. N. Chipanina, L. P. Oznobikhina, T. N. Aksamentova, A. R. Romanov, A. Y. Rulev, *Tetrahedron* **2014**, *70*, 1207.
[17] P. Subramaniam, C. Ramasubbu, S. Athiramu, *Green Chem.* **2017**, *19*, 2541.
[18] V. Y. Sosnovskikh, B. I. Usachev, *Mendeleev Commun.* **2000**, *10*, 240.
[19] CrysAlisPro, Oxford Diffraction Ltd., **2009**.
[20] G. M. Sheldrick, *SHELXS-97: Program for Crystal Structure Resolution*, University of Göttingen, Göttingen, Germany **1997**.
[21] L. J. Farrugia, *J. Appl. Crystallogr.* **1997**, *30*, 565.
[22] C. F. Macrae, I. J. Bruno, J. A. Chisholm, P. R. Edgington, P. McCabe, E. Pidcock, L. Rodriguez-Monge, R. Taylor, J. van de Streek, P. A. Wood, *J. Appl. Crystallogr.* **2008**, *41*, 466.
[23] M. J. Frisch, G. W. Trucks, H. B. Schlegel, G. E. Scuseria, M. A. Robb, J. R. Cheeseman, J. A. Montgomery Jr., T. Vreven, K. N. Kudin, J. C. Burant, J. M. Millam, S. S. Iyengar, J. Tomasi, V. Barone, B. Mennucci, M. Cossi, G. Scalmani, N. Rega, G. A. Petersson, H. Nakatsuji, M. Hada, M. Ehara, K. Toyota, R. Fukuda, J. Hasegawa, M. Ishida, T. Nakajima, Y. Honda, O. Kitao, H. Nakai, *Gaussian 03*, Gaussian Inc., Pittsburgh, PA **2003**.
[24] A. D. Becke, *Density-Functional Thermochemistry. III. The Role of Exact Exchange*, AIP, New York **1993**.
[25] C. Lee, W. Yang, R. G. Parr, *Phys. Rev. B* **1988**, *37*, 785.
[26] J. P. Perdew, K. Burke, M. Ernzerhof, *Phys. Rev. Lett.* **1996**, *77*, 3865.
[27] M. J. Turner, J. J. McKinnon, S. K. Wolff, D. J. Grimwood, P. R. Spackman, D. Jayatilaka, M. A. Spackman, *CrystalExplorer17*, University of Western Australia, Crawley, Australia **2017**.
[28] J. J. McKinnon, M. A. Spackman, A. S. Mitchell, *Acta Crystallogr., Sect. B: Struct. Sci., Cryst. Eng. Mater.* **2004**, *60*, 627.
[29] J. J. McKinnon, D. Jayatilaka, M. A. Spackman, *Chem. Commun.* **2007**, 3814.
[30] M. A. Spackman, D. Jayatilaka, *CrystEngComm* **2009**, *11*, 19.
[31] M. A. Spackman, *Chem. Rev.* **1992**, *92*, 1769.
[32] P. Gilli, V. Bertolasi, V. Ferretti, G. Gilli, *J. Am. Chem. Soc.* **2000**, *122*, 10405.
[33] S. J. Grabowski, W. A. Sokalski, J. Leszczynski, *Chem. Phys.* **2007**, *337*, 68.
[34] R. J. Baker, P. E. Colavita, D. M. Murphy, J. A. Platts, J. D. Wallis, *J. Phys. Chem. A* **2012**, *116*, 1435.
[35] T. V. Rybalova, I. Y. Bagryanskaya, *J. Struct. Chem.* **2009**, *50*, 741.
[36] P. E. Hansen, J. Spanget-Larsen, in *The Chemistry of Phenols* (Ed: Z. Z. Rappoport), Wiley, Chinchester, UK **2003**.
[37] F. Hibbert, J. Emsley, D. Bethell, in *Advances in Physical Organic Chemistry*, Academic Press, Cambridge, MA **1991**, p. 255.
[38] H. Rostkowska, M. J. Nowak, L. Lapinski, L. Adamowicz, *Phys. Chem. Chem. Phys.* **2001**, *3*, 3012.
[39] M. V. Korolevich, V. V. Sivchik, N. A. Matveeva, R. G. Zhbankov, V. A. Lastochkina, M. L. Frenkel, A. I. Ladut'ko, A. V. Pavlov, E. P. Petryaev, *J. Appl. Spectrosc.* **1987**, *46*, 400.
[40] A. L. Verma, *Spectrochim. Acta, Part A* **1971**, *27*, 2433.
[41] V. Krishnakumar, V. Balachandran, *Spectrochim. Acta, Part A* **2005**, *61*, 2510.
[42] A. Belay, *Food Chem.* **2010**, *121*, 585.